

Article

Finite Element and Neural Network Models to Forecast Gas Well Inflow Performance of Shale Reservoirs

Reda Abdel Azim ^{1,*} and Abdulrahman Aljehani ² ¹ Petroleum Engineering Department, American University of Kurdistan, Sumel 42003, Iraq² Faculty of Earth Sciences, King Abdulaziz University, Jeddah 21589, Saudi Arabia

* Correspondence: reda.abdulrasoul@auk.edu.krd

Abstract: Shale gas reservoirs are one of the most rapidly growing forms of natural gas worldwide. Gas production from such reservoirs is possible by using extensive and deep well fracturing to contact bulky fractions of the shale formation. In addition, the main mechanisms of the shale gas production process are the gas desorption that takes place by diffusion of gas in the shale matrix and by Darcy's type through the fractures. This study presents a finite element model to simulate the gas flow including desorption and diffusion in shale gas reservoirs. A finite element model is used incorporated with a quadrilateral element mesh for gas pressure solution. In the presented model, the absorbed gas content is described by Langmuir's isotherm equation. The non-linear iterative method is incorporated with the finite element technique to solve for gas property changes and pressure distribution. The model is verified against an analytical solution for methane depletion and the results show the robustness of the developed finite element model in this study. Further application of the model on the Barnett Shale field is performed. The results of this study show that the gas desorption in Barnett Shale field affects the gas flow close to the wellbore. In addition, an artificial neural network model is designed in this study based on the results of the validated finite element model and a back propagation learning algorithm to predict the well gas rates in shale reservoirs. The data created are divided into 70% for training and 30% for the testing process. The results show that the forecasting of gas rates can be achieved with an R^2 of 0.98 and an MSE = 0.028 using gas density, matrix permeability, fracture length, porosity, PL (Langmuir's pressure), VL (maximum amount of the adsorbed gas (Langmuir's volume)) and reservoir pressure as inputs.

Keywords: Langmuir; shale; gas; neural; finite element

Citation: Abdel Azim, R.; Aljehani, A. Finite Element and Neural Network Models to Forecast Gas Well Inflow Performance of Shale Reservoirs. *Processes* **2022**, *10*, 2602. <https://doi.org/10.3390/pr10122602>

Academic Editors: Tianshou Ma and Yuqiang Xu

Received: 3 November 2022

Accepted: 29 November 2022

Published: 5 December 2022

Publisher's Note: MDPI stays neutral with regard to jurisdictional claims in published maps and institutional affiliations.



Copyright: © 2022 by the authors. Licensee MDPI, Basel, Switzerland. This article is an open access article distributed under the terms and conditions of the Creative Commons Attribution (CC BY) license (<https://creativecommons.org/licenses/by/4.0/>).

1. Introduction

Recently, shale gas reservoirs have been considered essential resources, used to supply the world with part of the required energy to compensate for the depletion of conventional reservoirs. Shale gas reservoirs are not similar to conventional reservoirs; these types of formations include conductive natural fractures, narrow thickens and infinite lateral extension. As a result of these properties, only horizontal wells are usually used to increase the gas production rates. In addition, such reservoirs typically have ultra-low permeability; therefore, hydraulic fracturing technology is used to exploit the production zones by creating fracture networks around the wellbore. The gas stored in shale reservoirs is in both free and adsorbed phases; consequently, the production behavior drastically changes through the reservoir's lifetime [1–3].

Based on different field and lab data, 50% of gas in place is stored as adsorbed gas [4,5] and this amount is quantified through Langmuir isotherms [6–11]. The Langmuir isotherms are always used to describe the relationship between methane adsorption on shale surface and gas pressure through ignoring the variation in reservoir temperature.

The gas adsorption in shale systems is controlled by the TOC (Total Organic Carbon), organic matter type, clay minerals and thermal maturity. As the TOC content is raised, the

gas capacity increases. The presence of gas in shale in micro-fractures and on surface shale grains during the gas production process leads to gas releasing that provides additional gas in place. Gas production takes place by diffusion in shale matrices while it takes place by Darcy's flow type in the fractures [12–17]. Due to the extra low permeability of shale formations, the continuous effects of pressure transients during well production complicate the gas production forecasting process. Hence, this study presents a simulation model to estimate the shale gas volume in place and to predict surface gas flow rates.

During the production process, free gas is produced at the beginning from natural fractures, then the matrix feeds the fracture network. In turn, the matrix is fed by adsorbed gas existing in the nanopores. In the presented simulation model in this study, organic matter is assumed to be located in the matrix while inorganic matters (free gas) are stored in the micro-fractures. The model also based on the assumption that the gas desorption from organic matter feeds the matrix only, and never contacts the fracture directly, in which the gas flows out of the fractures and not from matrix in a direct way. A vertical well is used in the simulation model for the production process through a horizontal hydraulic fracture.

In this study, the Langmuir's isotherm is used to define the relationship between the gas storage capacity and pressure of the reservoir, and it could be given by:

$$V_E = V_L \frac{P}{P + P_L} \quad (1)$$

where V_E is the gas content, P is the reservoir pressure, P_L is the Langmuir's pressure and V_L is the maximum amount of the adsorbed gas (Langmuir's volume).

The gas content (V_E) in the reservoir rock is affected by several factors including mineral composition and organic matter. The organic matter is considered more important than the mineral composition as it controls the amount of surface area available for adsorption. The organic matter's features include total organic carbon content (TOC) and thermal maturity, and the Langmuir's volume is a function of both. In the shale gas production process, gas desorption cannot be ignored because at low reservoir pressures, most of the gas production comes from desorbed gas. The desorption is the reverse process of adsorption and with a decline in reservoir pressure and production of free gas, the adsorbed gas desorbs from the matrix surface to preserve the reservoir equilibrium and ensure that the reservoir pressure is maintained for a long period. The desorption process starts when the reservoir pressure falls below critical desorption pressure [18,19]. The rate of desorbed gas is controlled by the reservoir permeability, and it has a significant effect on the surface gas production rate.

The desorbed gas volume can be defined by:

$$V_{des} = V_L V_b \rho_R \frac{P}{P + P_L} \quad (2)$$

where V_b is reservoir bulk volume and ρ_R is the shale density at initial reservoir pressure.

The desorbed gas rate into the matrix pore space can be given by:

$$-\frac{\partial V_{des}}{\partial t} = -V_L V_b \rho_R \frac{1}{(P + P_L)^2} \frac{\partial P}{\partial t} \quad (3)$$

This equation gives the volumetric rate in scf/sec and the negative sign indicates that the adsorbed gas decreases as gas desorbs into the matrix.

The advancement in drilling in shale reservoirs for petroleum production using hydraulic fracturing has become a major energy resource worldwide. Such an advancement requires an accurate petroleum production forecast due to the high cost of these technologies. This concern has led scientists around the world to search for an economically feasible project to accurately estimate petroleum production from such reservoirs.

Hydraulic fracturing parameters are the main controlling factor to accurately predict shale gas production and have attracted scientists to develop prediction models. A response

surface methodology (RSM) model was proposed by Yu and Sepehrnoori [20] to estimate the net present value (NPV) of a shale gas project. The authors used reservoir parameters and petrophysical properties such as porosity, permeability, reservoir pressure and thickness and fracture properties (spacing, conductivity, half length). The authors did not include a crucial parameter in determining the initial gas in place, namely the initial gas saturation and adsorbed gas content. Later, Nguyen-Le et al. [21] used the parameters investigated by [20], the initial gas saturation and adsorbed gas content to develop an economic indicator for the evaluation of shale gas production potential. In their model, they assumed that hydraulic fracturing generates planner fractures. However, in naturally fractured reservoirs, hydraulic fracturing may activate the existing natural fracture system [22–26].

The advancement of artificial neural networks (ANN) for optimizing and predicting petroleum production from shale reservoirs has encouraged scientists to use the technology to accurately predict production. Kim et al. [27] used eleven hydraulic fractures as well as reservoir parameters to predict shale gas production. The authors used matrix-fracture coupling and the diffusion coefficient as input controlling parameters for the prediction model, while these parameters have no direct impact on shale gas production. Furthermore, the authors, similar to Yu and Sepehrnoori [20], ignored the initial gas saturation and adsorbed gas content. Li and Han [28] developed an ANN model to predict the pressure decline parameter using fracture and reservoir properties. The predicted parameters along with the logistic growth decline curve model can be used to reconstruct a production profile. On the other hand, the authors collected the data from vertical oil wells which induce a single stage longitude fracture to predict the model [29]. Multi-stage fracturing techniques are usually carried out in a horizontal well where it is divided into many stages. Moreover, each fracture stage is further divided into more than one fracture cluster. This technique helps in increasing the productivity and contact area between the reservoir and wells. Hence, the predicted model highly depends on the type of wells (i.e., vertical or horizontal).

One model widely used in the literature to predict the petroleum production profile is the decline curve analysis (DCA), due to its simplicity and efficiency. The principle of DCA is to fit the production history data by tuning its decline parameters until the error between the predicted and real data is minimized. Once the minimum fitting error is reached, the DCA model, along with a set of decline parameters, is used to predict future production. One important parameter for accurate prediction of the DCA model is the availability of large amounts of production data (i.e., time). Nelson et al. [30] used the DCA model to predict shale gas production from 48 months of production data. Bashier [31] and Zuo et al. [32] predicted shale gas production using the DCA model with a minimum of 60 months of production history. Odi et al. [33] predicted shale gas production using the DCA model with 36 months of production history. It can be noted from the previous studies that the average production time used for shale gas production predictions ranges from 3–5 years.

Therefore, this study presents an accurate numerical simulation model to estimate the gas production rate and gas volume in place for both adsorbed and free gas. The model is based on a finite element technique using 8-node quadrilateral elements. The gas flow equations are generated by using continuity and Darcy's equations. In addition, an artificial neural network model is proposed to develop a novel correlation for predicting the gas rate and inflow performance using the proposed simulation finite element model. The developed correlation is based on numerous inputs including gas density, matrix permeability, fracture length, porosity, PL (Langmuir's pressure), VL (maximum amount of the adsorbed gas (Langmuir's volume)) and reservoir pressure. This novel correlation will be used in assessing gas shale production avoiding the complexity existing in simulation models.

2. Description of the Flow Simulation Model

A mathematical model is derived in this study to simulate gas flow in shale reservoirs. The gas is considered in a free state in the porous media and adsorbed in the shale matrix.

The model is developed for single-phase fluid flow in a 2-dimensional space. In the developed mathematical model, gas is produced under constant bottomhole pressure. The gas flows from the matrix to the horizontal fracture and directly to the vertical well.

The continuity equation is used as follows:

$$\frac{\partial}{\partial x}(\rho_g u_g) = -\frac{\partial}{\partial t}(\phi \rho_g) \quad (4)$$

where ρ_g is the gas density and u_g is the gas velocity.

The continuity equation can be written in terms of formation volume factor as:

$$\frac{\partial}{\partial x}(\beta_g u_g) - q_g = -\frac{\partial}{\partial t}(\phi \beta_g) \quad (5)$$

where q_g is the source/sink and;

$$u_g = -\frac{ck_x}{\mu_g} \frac{\partial p_g}{\partial x} \quad (6)$$

where c is the conversion factor, k_x is the formation permeability in mD, μ_g is the gas viscosity and p_g is the gas pressure.

By introducing Darcy's velocity in Equation (4), the equation can be written as:

$$\frac{\partial}{\partial x} \left(\frac{ck_x \beta_g}{\mu_g} \frac{\partial p_g}{\partial x} \right) + q_g = \phi \frac{\partial p_g}{\partial t} \frac{\partial \beta_g}{\partial p_g} \quad (7)$$

In case of two-dimensional flows, the equation will be:

$$\frac{\partial}{\partial x} \left(\frac{ck_x \beta_g}{\mu_g} \frac{\partial p_g}{\partial x} \right) + \frac{\partial}{\partial z} \left(\frac{ck_z \beta_g}{\mu_g} \frac{\partial p_g}{\partial z} \right) + q_g = \phi \frac{\partial p_g}{\partial t} \frac{\partial \beta_g}{\partial p_g} \quad (8)$$

The amount of adsorbed gas can be treated as a sources term (injection well); therefore, by using Equations (3) and (8), it can be written as:

$$\frac{\partial}{\partial x} \left(\frac{ck_x \beta_g}{\mu_g} \frac{\partial p_g}{\partial x} \right) + \frac{\partial}{\partial z} \left(\frac{ck_z \beta_g}{\mu_g} \frac{\partial p_g}{\partial z} \right) + V_L \rho_R \frac{1}{(p + p_L)^2} \frac{\partial p}{\partial t} = \phi \frac{\partial p_g}{\partial t} \frac{\partial \beta_g}{\partial p_g} \quad (9)$$

Introducing a weak formulation, Equation (6) for fluid flow through matrix is described as follows:

$$\int_{\Omega} \mathbf{w} \phi \frac{\partial B_g}{\partial t} d\Omega = \int_{\Omega} \mathbf{w} \left(\frac{\partial}{\partial x} \left(\frac{ck_x B_g}{\mu} \frac{\partial p}{\partial x} \right) + \frac{\partial}{\partial z} \left(\frac{ck_z B_g}{\mu} \frac{\partial p}{\partial z} \right) \right) d\Omega + \int_{\Gamma} \mathbf{w}^T q d\Gamma \quad (10)$$

where ($\mathbf{w} = \mathbf{w}(x, y, z)$) is a trial function.

Using the finite element method for discretization with respect to time and space results in:

$$\begin{aligned} & \int_{\Omega} (\phi c_t N_p^T N_p d\Omega) \left(\vec{P}^i - \vec{P}^{i-1} \right) + \left(V_L \rho_R \frac{1}{(p + p_L)^2} N_p^T N_p d\Omega \right) \left(\vec{P}^i - \vec{P}^{i-1} \right) \\ & + \Delta t^i \left[\int_{\Omega} \left(\frac{ck_x B_g}{\mu_g} \frac{\partial N_p^T}{\partial x} \frac{\partial N_p}{\partial x} + \right) d\Omega \right] \vec{P}^i + \Delta t^i \left[\int_{\Omega} \left(\frac{ck_z B_g}{\mu_g} \frac{\partial N_p^T}{\partial z} \frac{\partial N_p}{\partial z} \right) d\Omega \right] \vec{P}^i \\ & + \int_{\Gamma} N_p^T \mathbf{q} d\Gamma = 0.0 \end{aligned} \quad (11)$$

where:

$$\vec{P}^T = (p_1 \ p_2 \ \dots \ p_n) \quad (12)$$

$$\vec{N}_p^T = (N_1 \ N_2 \ \dots \ N_n) \quad (13)$$

$$\vec{N}_u = \begin{bmatrix} N_1 & 0 & N_2 & \dots & 0 \\ 0 & N_1 & 0 & \dots & N_N \end{bmatrix} \quad (14)$$

where N_p and N_u are the shape function for pressure and displacement, respectively, n is the number of nodes, Γ is the domain boundary and P is pressure nodal value.

Galerkin's finite element method is used to discretize the equations as follows:

$$A.(p) + s.(p) + H.(p) = 0 \quad (15)$$

where:

$$A = \int_{ve} [B]^T \left(k \frac{P_L}{(P_L + P)^2} \right) N_p dV \quad (16)$$

$$S = \int_{ve} [N_p]^T \left(\frac{\beta_g V_L P_L}{(P_L + P)^2} \right) N_p dV \quad (17)$$

$$H = \int_{ve} [\nabla N_p]^T \left(\frac{k}{\mu_g} \right) \nabla N_p dV \quad (18)$$

3. Validation of the Numerical Model

Figure 1 shows the model geometry with different boundary conditions. The inner boundary of the reservoir is set to a wellbore pressure of 1000 psi while the outer boundary condition is set as no flow boundary, ignoring the minimum and maximum horizontal stresses. The well is vertical with one hydraulic fracture used to exploit the gas stored. A plain strain is assumed in this model and this assumption is valid when one of the dimensions is very large when compared to other two. In order to validate the developed numerical simulator, a 2-D finite element mesh is used with 5000 elements and eight nodes (see Figure 2). The mesh is generated with a fracture intersecting the wellbore. The fracture length is 100 ft and the parameters of the 2-D model used for the simulation are presented in Table 1. The reservoir pressure is set as 5500 psi with very low permeability of 0.01 md to simulate the actual conditions in shale reservoirs.

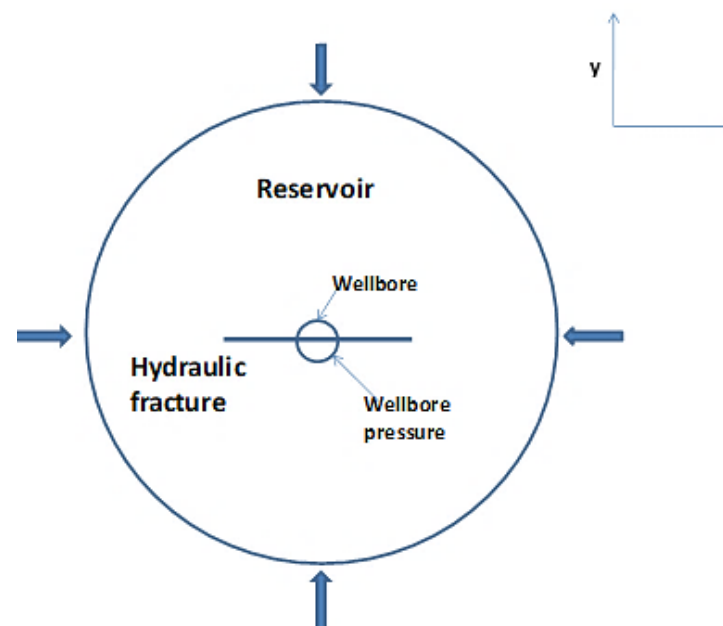


Figure 1. Schematic of the fracture reservoir used for production model.

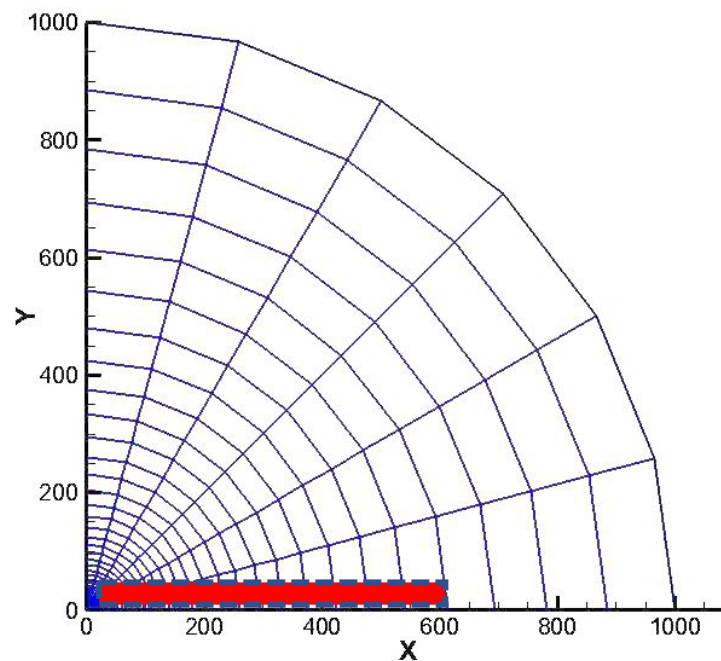


Figure 2. 2-D mesh used for the validation of the numerical model developed in this study.

Table 1. Parameters used in the verification of the developed numerical model.

Parameter	Value
Langmuir's volume	0.08 scf/lb
Langmuir's pressure	5100 psi
Gas viscosity	0.01 cp
Gas density	6 lb/cf
Fracture length	1 m
Fracture permeability	500 md
Initial reservoir pressure	5500 psi
Wellbore pressure	1000 psi
Formation permeability, k_x	0.01 md
Formation permeability, k_y	0.01 md
Wellbore radius	0.1 m
Reservoir outer radius	1000 m

Only a one-quarter model is selected to take advantage of the reservoir symmetry as shown in Figure 2. Figure 3 shows in detail the gas distribution pressure inside the fracture and the shale matrix. It can be seen from Figure 3 that the gas pressure is initially depleted inside the hydraulic fracture; consequently, pressure depletion occurs on the matrix surface. Figure 4 shows the comparison between the analytical and numerical solution for the gas pressure distribution inside the matrix and the hydraulic fracture. It can be seen from these figures that the gas pressure changes with production time across the wellbore to the reservoir boundary are in a good agreement with the analytical solution. Hence, the developed model in this study can be used to address numerous problems in gas shale reservoirs.

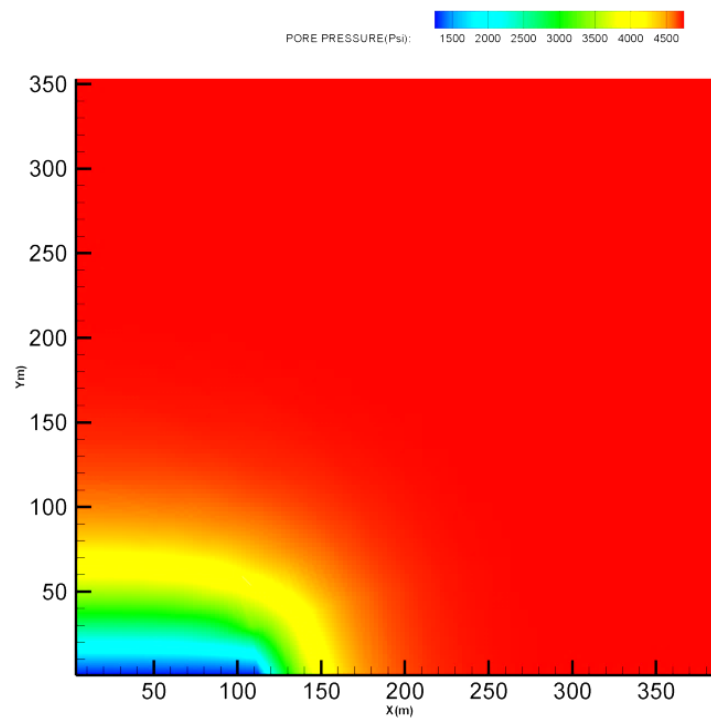


Figure 3. The gas pressure distribution around the wellbore and inside the fracture after 10 days of production for $P_i = 5500$ psi, $P_{wf} = 1000$ psi and $k=0.01$ md.

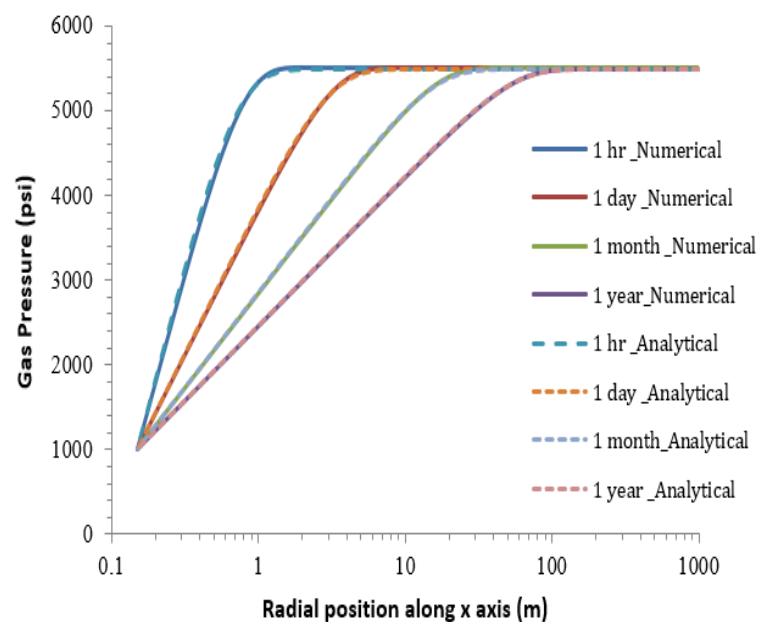


Figure 4. The comparison between analytical and numerical solution of shale gas pressure for $P_i = 5500$ psi, $P_{wf} = 1000$ psi and $k=0.01$ md.

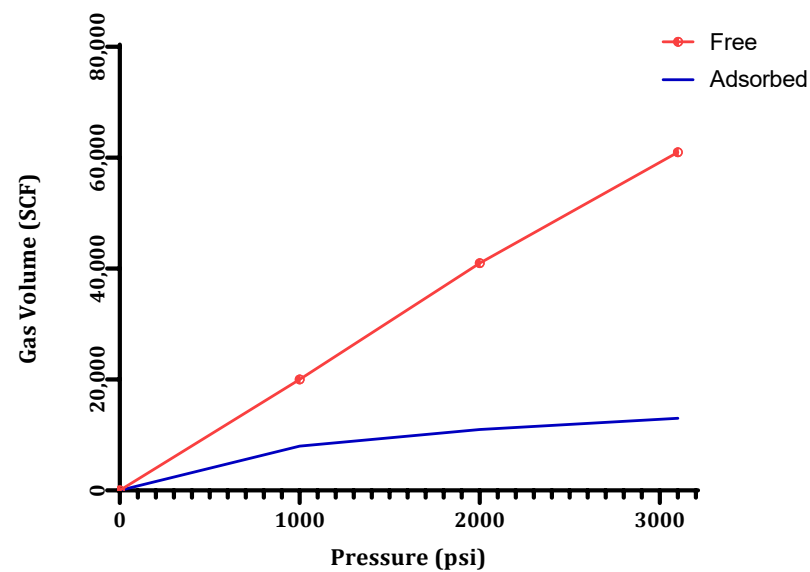
4. Results and Discussion

A case study is taken from Barnett Shale to estimate the volume of the reservoir adsorbed and free gas. In addition, the developed simulator in this study will evaluate the gas shale flow rates with time. A sensitivity study is performed as well to show the effect of various fluid properties on gas production rates. The collected data are presented in Table 2. The developed simulation model in this study assumes that the gas is stored in natural fractures and pores and it is adsorbed in organic matter.

Table 2. Shale gas reservoir properties used in the verification of the developed numerical model.

Parameter	Value
Gas viscosity	0.019 cp
Gas formation volume factor	1.35 scf/rcf
Langmuir's volume	0.099 scf/lb
Langmuir's pressure	2696 psi
Initial compressibility	$5.3 \times 10^{-5} \text{ psi}^{-1}$
Gas density	6.4/lb/cf
Fracture length	20 ft
Fracture permeability	500 md
Initial reservoir pressure	3100 psi
Wellbore pressure	2550 psi
Formation permeability, K_x	0.001 md
Formation permeability, K_y	0.001 md
Porosity	0.05
Reservoir outer radius	1000 m

Figure 5 shows the amount of the adsorbed and free gas versus the change in the reservoir pressure, calculated using the Langmuir's isotherm for Barnett Shale. As it can be seen from this figure, a significant amount of adsorbed gas exists in the 20 ft fracture used in the finite element mesh (see Figures 1 and 2).

**Figure 5.** Free gas and adsorbed gas content for Barnett Shale versus reservoir pressure.

Using the permeability of 0.001 md as homogenous reservoir property, the gas production profile is obtained, as shown in Figure 6. The gas production profile shows a long term well performance of 18 years, and this performance is required during the production process in shale gas reservoirs. The gas well is produced at constant bottom hole pressure of 2550 psi at the initial production stage. The free gas exists in the natural fracture and pores. The gas is produced continuously from the fracture until the pressure in the matrix reaches the critical desorption pressure. Then, the adsorbed gas feeds the porous area through the desorption process at a rate depending on the pressure change. Hence, the production rate stabilizes after certain period of production when the total amount of adsorbed gas is desorbed into the fracture near the wellbore (see Figure 6). The production rate is initially started with 180 scf/s and this value is very close to what has been estimated by Wang [34] (211 scf/s). The difference between this study's initial gas rate estimation and that of Wang [34] arises from the different geometry and fracture network used in the study by Wang [34].

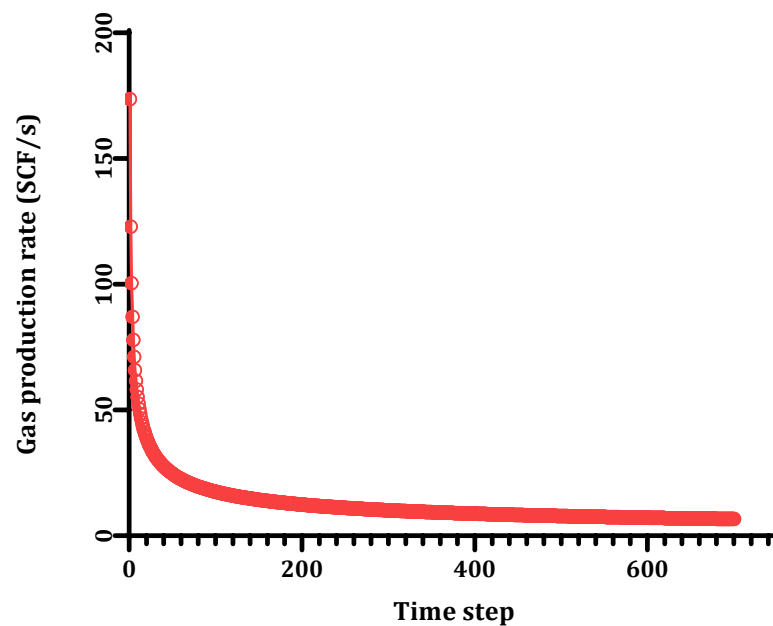


Figure 6. Gas production rate versus reservoir pressure.

Figure 7 shows the cumulative gas production. As it can be seen from Figure 7, the cumulative gas production is initially low due to small the time step size used at the beginning of the simulation run. Then the cumulative gas production volume increases with decreasing the pressure around the hydraulic fracture and the porous matrix. The total volume produced after 12 years of gas production is 80 MMSCF in comparison to the work of Wang [34], which found 88 MMSCF. Estimations of cumulative gas volume using this simulation study and the study of Wang [34] are in a good agreement. Wang [34] uses a sub-surface fracture network map which gives more gas volume during the production process.

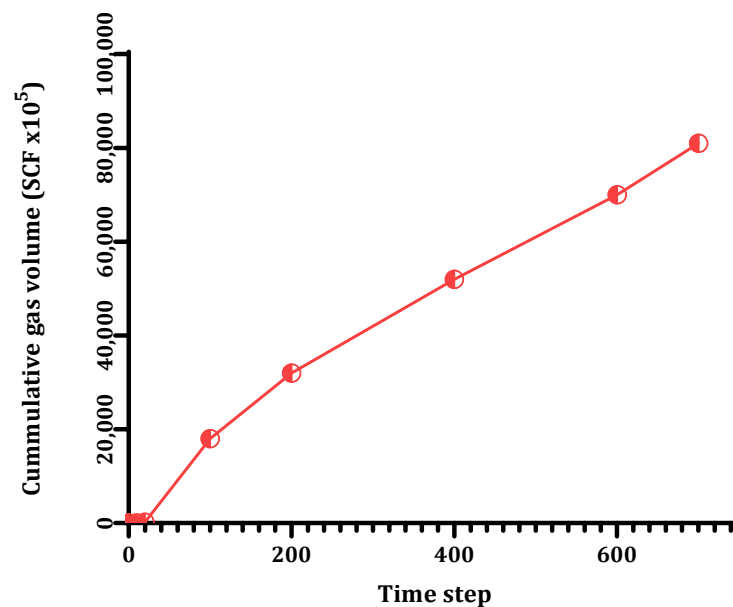


Figure 7. Barnett Shale cumulative gas production volume over 18 years.

Figure 8 shows the variation in gas pressure change due to gas production in two mesh elements, one is close to the wellbore and the other is far from the fracture and wellbore. Figure 8 shows various behaviors of the elements with time. In the early stages of the free gas production, the gas is produced from the cell/element near the wellbore and the closest

to the fracture. Hence, the pressure drop decreases faster (see Figure 8). Next, during the period of production, the pressure stabilizes due to it reaching the phase of critical gas desorption. However, the pressure in the cell/element far from the wellbore displays a slow rate of reduction due to low matrix permeability.

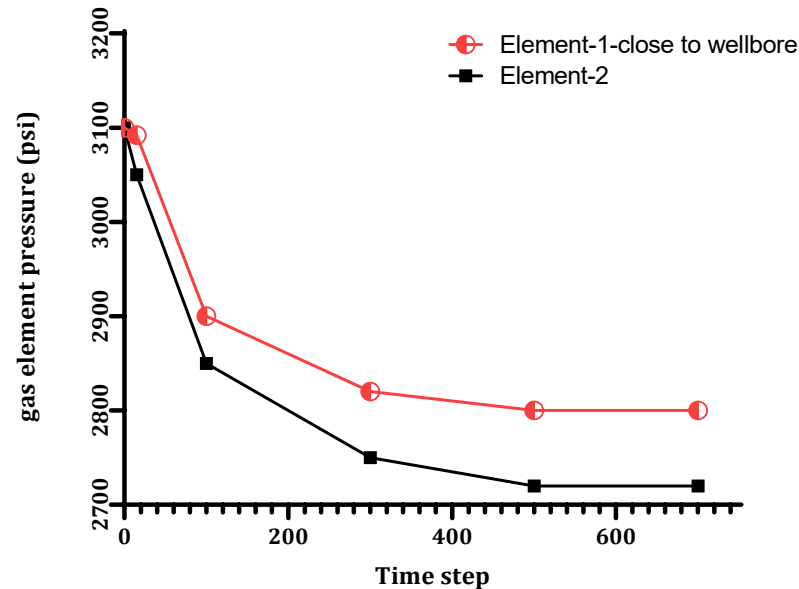


Figure 8. Pressure drop behavior for two elements used in the simulation model.

It can be observed from Figure 9 that the gas pressure diffusion behavior is transient within the hydraulic fracture and matrix at early production stage and reached the boundary after two months of production and the flow regime changed to a pseudo steady-state, dominant for the rest of reservoir production time.

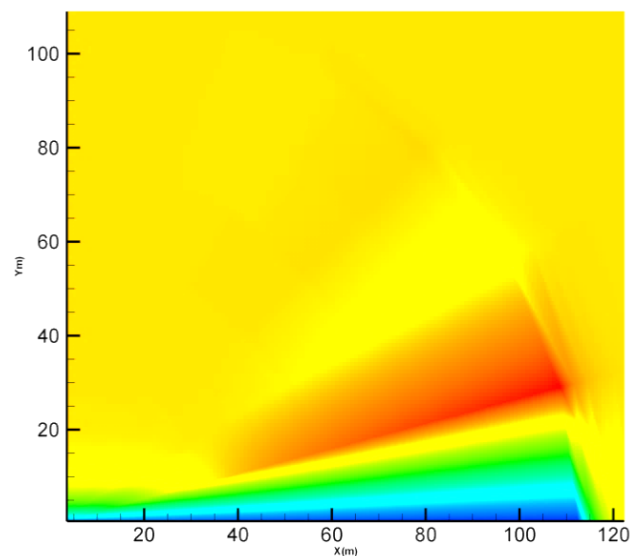


Figure 9. Gas pressure behavior at the early stage of the production process for $P_i = 3100$ psi, $P_{wf} = 2550$ psi, $k=0.001$ md and fracture length = 20 ft. The blue color is for $P = 2550$ psi and the red color is for $P = 3100$ psi.

Figure 10 shows the gas desorption volume for the two cells/elements (with an element/cell close to the fracture and another far from the wellbore). As it can be seen from Figure 10, the gas production starts in the element that is close to the wellbore; hence, its average pressure will be depleted faster. Next, the pressure in the adjacent

element will start to deplete to the critical gas desorption pressure. Afterwards, the cell will feed the gas to the pore space and this behavior depends on the reservoir heterogeneity. This means a different behavior might be observed in the desorption process due to a difference in permeability and porosity of the elements.

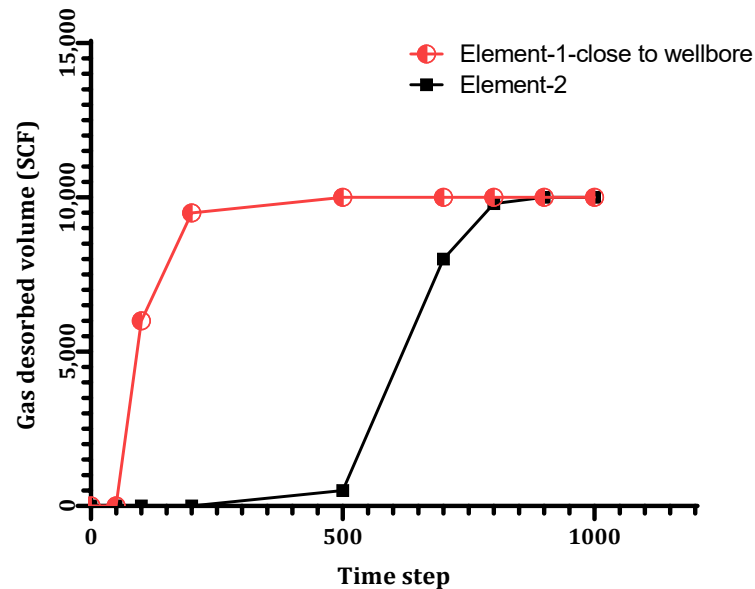


Figure 10. Gas desorbed volume for two elements used in the simulation model.

A sensitivity study was performed to test the effect of the fracture length on the gas production rates. The fracture lengths used were 20 ft and 60 ft. Figure 11 shows the production profile in both cases (with fracture lengths of 20 and 60 ft). It can be seen from Figure 11 that a low production rate profile with fracture length = 20 ft occurred. In addition, the critical desorption pressure is achieved at a later stage for fracture with a length = 60 ft. It can be observed from Figure 11 that the gas production rate is sustained for a long period during the production process with a fracture length = 60 ft. Moreover, it can be observed from Figure 11 that the gas production rate declines 20–35% per month at the beginning of the production process and then the declining rate stabilizes at around 7% after 2 years of production (100-time step) which is a typical scenario for unconventional reservoirs.

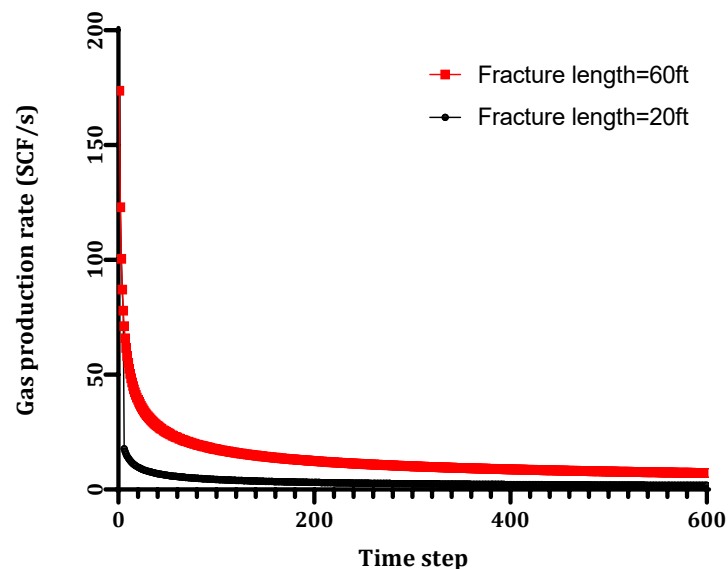


Figure 11. Comparison between production profiles for different fracture lengths.

Since the amount of adsorbed gas depends on the gas density, a simulation run is performed under different gas densities of 5 and 25 lb/cf, respectively. The analysis in Figure 12 shows that the gas production profile is sustained longer in the case of a higher gas density, as the gas in this case is densely packed into the organic matter; thus, a higher amount of adsorbed gas will exist. Therefore, production of more gas is expected with a high gas density and this parameter will be taken as an essential input parameter in the ANN model to develop a new correlation for gas rate prediction.

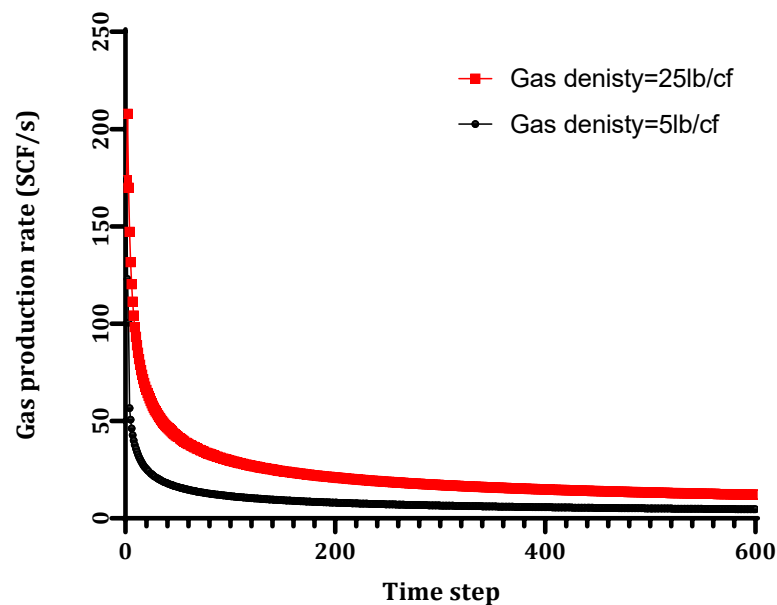


Figure 12. Comparison between production profiles for different gas densities.

5. Neural Network for Gas Rate Prediction

Numerous machine learning algorithms have been used to predict the gas well performance in shale reservoirs. Li et al. [35] used the Neural Based Decision Tree (NDT) learning model for gas production prediction where ANN outperformed NDT. Clarke et al. [36] used a high order neural network for gas well rate forecasting, while Klie [37] used surrogate models for well rate forecasting. Fulford et al. [38] combined a supervised learning algorithm with calibrated bias to improve the posterior distribution of forecasts.

Nguyen [39] used the various fracture and reservoir properties to predict the production decline parameters by developing an ANN model. The ANN model was based on data collected from fractured vertical wells which induce a single-stage longitudinal fracture. Syed et al. [40,41] used the unsupervised machine learning algorithm to model and analyze the shale gas production.

Numerous authors have used machine learning algorithms including the neural network (ANN), random forest (RF), function networks (FNs), adaptive neuro-fuzzy inference system (ANFIS) and support vector machine (SVM) to predict the gas shale rates during the production process [42,43].

The back propagation (BP) learning algorithm was used in this study as a supervised algorithm. During the backward propagation, the errors are sent backward through the hidden and input layers. Then, the error values are used to update the weight in the artificial neural network (ANN). The error value at the output neuron can be defined as a quadratic cost function:

$$E_p = \frac{1}{2} \sum_1^{n_2} (x_p - y_p)^2 \quad (19)$$

where E is the error vector for the training pattern p .

A gradient decent method [44,45] is used in this study in order to modify the weight of the connection and compute the delta weight vector to minimize the cost function. A stopping criterion is set in the ANN for a fixed error threshold, for a fixed number of allowable epochs and for the use of validation data [46–48]. These criteria are very sensitive to the input parameters and if these parameters are not chosen properly, the results will show poor performance due to excessive training. Notably, the target outputs in the training are usually scaled in the interval of (0 and 1) for logistic function.

During the learning phase, it is mandatory to test the performance of the neural net at each single epoch. Therefore, the mean square error *MSE* in Equation (20) is used to show the network performance.

$$MSE = \sqrt{\frac{\sum_1^{n_1} \sum_1^{n_2} (x_p - y_p)^2}{n_1 \cdot n_2}} \quad (20)$$

where n_1 and n_2 are number of training output neurons, respectively. x_p and y_p are the target and calculated outputs, respectively.

This section will show how the validated simulator developed in this study is used to construct the ANN model by creating almost 300 data points to be used in the training and testing processes. The inputs include gas density, matrix permeability, fracture length, porosity, PL (Langmuir's pressure), VL (maximum amount of the adsorbed gas (Langmuir's volume)) and reservoir pressure. The target output is the gas production rate (see Figure 13).

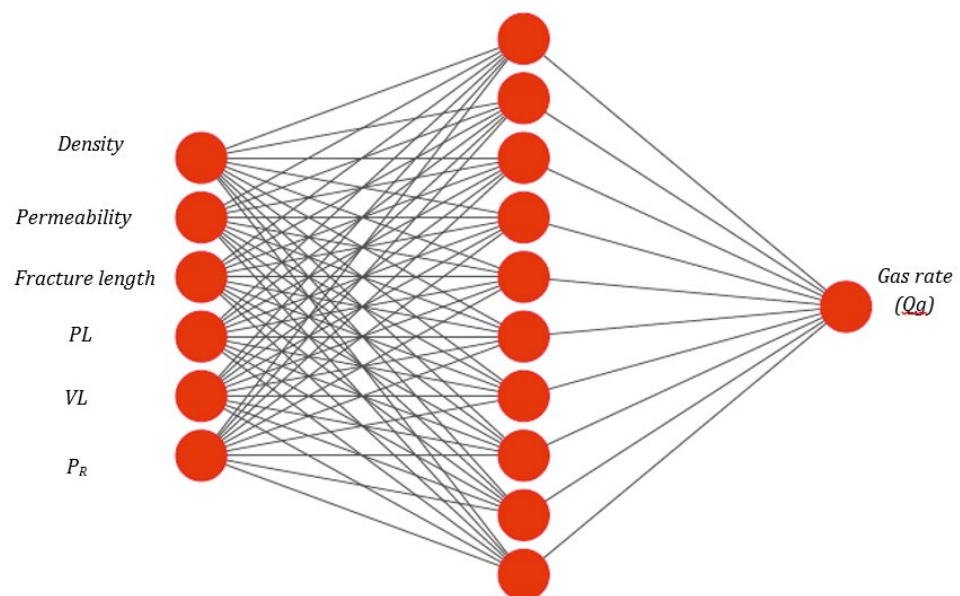


Figure 13. Artificial neural network architecture used in this study.

Date Description

Around 300 points are created using the validated finite element model in this study to design and develop the ANN model. The data contains six inputs including gas density, matrix permeability, fracture length, porosity, PL (Langmuir's pressure), VL (maximum amount of the adsorbed gas (Langmuir's volume)) and reservoir pressure that are used in the training process, while the output is the gas production rate. The statistical analysis of the collected data is presented in Table 3.

The data set is divided into two groups for training and testing processes. A total of 70% is assigned for the training and 30% for the testing. The Back Propagation learning algorithm is used to minimize the results error between actual and target outputs with the log sigmoid function. The BP learning algorithm provides exceptional results with an R^2 of

0.98 and a MSE = 0.018 for training (see Figure 14), and an $R^2 = 0.99$ for the testing process (see Figure 15).

Table 3. Statistics analysis of the input data.

Parameter	Gas Density (lb/cf)	Matrix Permeability (md)	Fracture Length (ft)	Langmuir's Volume (VL, psi)	Langmuir's Pressure (PL, psi)	Reservoir Pressure (psi)
Max	18	0.099491	60	0.099662	2795	3996
Min	4	6.08×10^{-5}	10	0.000322	701	1002
Standard Deviation	4.211135	0.028379	14.31894	0.028638	608.8278	866.6465
Skewness	-0.04798	-0.10025	-0.18278	-0.00804	0.010806	0.038504
Mean	11	0.053936	38	0.050758	1760	2446

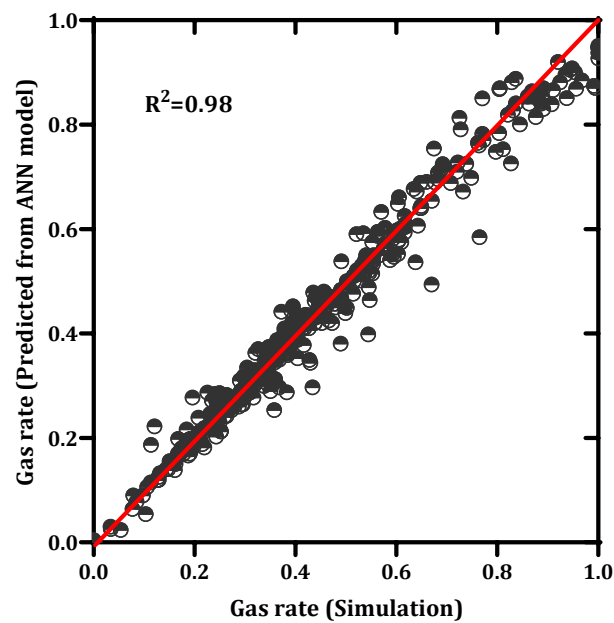


Figure 14. The predicted Q_g from ANN versus simulation results for training.

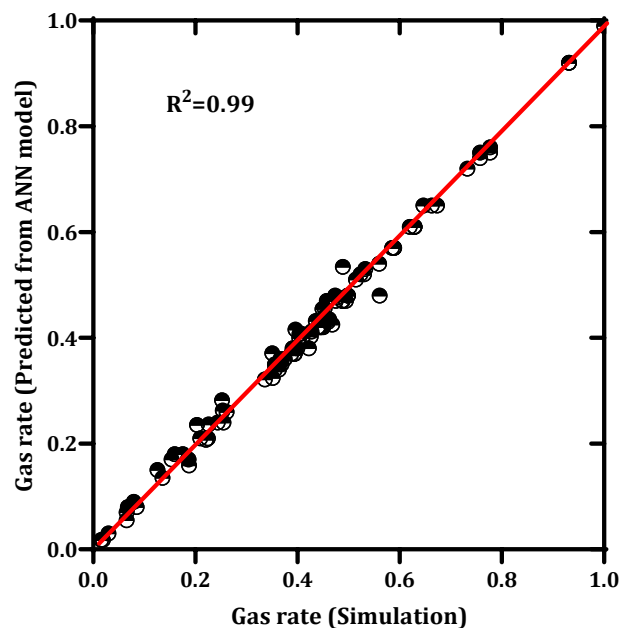


Figure 15. The predicted Q_g from ANN versus simulation results for testing.

Using the results of training and testing processes, a mathematical correlation is produced to show the relationship between the Q_g and inputs to be used in the forecasting of shale gas rates.

The novel correlation generated using ANN for Q_g estimation is given by:

$$Q_{gn} = \left[\sum_{i=1}^N w_{2i} \tan sig \left(\sum_{j=1}^J w_{1i,j} x_j + b_{1j} \right) \right] + b_2 \quad (21)$$

$$Q_{gn} = \left[\sum_{i=1}^N w_{2i} \left(\frac{1}{1 + \exp^{-(Gas\ density \times w_{1,j,1} + Frac/L \times w_{1,j,2} + K_{mat} \times w_{1,j,3} + V_L \times w_{1,j,4} + P_L \times w_{1,j,5} + P_R \times w_{1,j,6}) + b_1}} \right) \right] + b_2 \quad (22)$$

where Q_{gn} is the normalized gas rate, ($w_{2,i}$) is the vector weight between the hidden layer and output layer, ($w_{1,j}$) is the vector weight connecting the input and the hidden layer, j is the neuron number, b_1 is the biases vector for the input layer and b_2 for the output layer. The extracted Q_g equation can be attained by de-normalizing Q_{gn} as follows:

$$Q_g = 160 \times Q_{gn} + 12 \quad (23)$$

Table 4 shows the weights and bias for the correlation. The proposed correlation in Equation (22) can be used to estimate and predict the gas flow rate for the shale reservoirs using the above-mentioned inputs. Figure 16 shows the comparison between the simulated gas rates and the gas rates values extracted from the ANN model based on inputs. It can be seen from Figure 16 that a good match is achieved with a minimum square error (MSE) of 0.018. The correlation proves that the designed ANN model is reliable and helps in reducing the computational time used by the numerical simulation model which requires extensive mathematics knowledge.

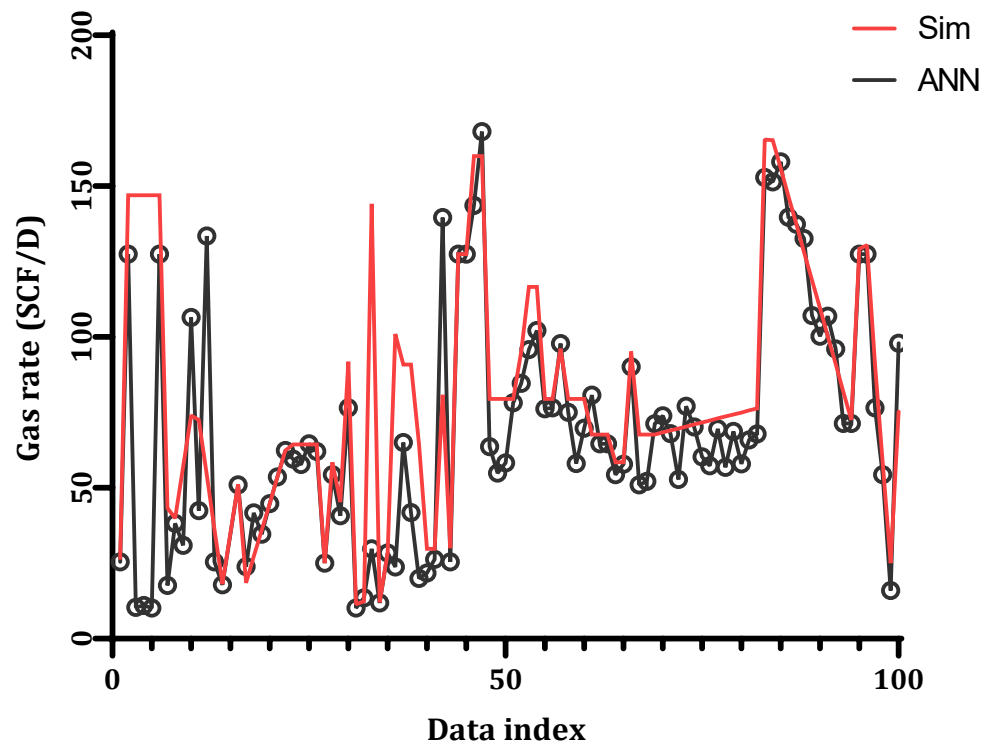


Figure 16. ANN gas flow rate vs. simulated gas flow rate.

Table 4. Weights and biases for the generated correlation Equation (22).

Neuron Number	Input and Hidden Layers Weights (w_1)						Hidden and Output Layers Weights (w_2)	Hidden Layer Bias (b_1)	Output Layer Bias (b_2)
1	$-1.34 \times 10^{+00}$	$-1.53 \times 10^{+00}$	1.04×10^{-01}	4.56×10^{-01}	$1.04 \times 10^{+00}$	$-2.73 \times 10^{+00}$	$-1.99 \times 10^{+00}$	4.93×10^{-02}	-0.4621008
2	8.02×10^{-01}	-3.40×10^{-01}	6.41×10^{-01}	1.31×10^{-01}	-5.66×10^{-01}	2.98×10^{-01}	$-2.53 \times 10^{+00}$	$-1.57 \times 10^{+01}$	
3	3.86×10^{-01}	8.12×10^{-01}	-1.18×10^{-01}	-6.67×10^{-02}	-2.47×10^{-01}	$-1.99 \times 10^{+00}$	9.62×10^{-02}	$-2.92 \times 10^{+00}$	
4	-4.72×10^{-01}	7.89×10^{-02}	-3.63×10^{-02}	1.10×10^{-01}	-7.36×10^{-02}	$1.35 \times 10^{+00}$	4.07×10^{-01}	3.42×10^{-01}	
5	-1.07×10^{-01}	2.10×10^{-01}	1.04×10^{-01}	2.09×10^{-01}	2.59×10^{-01}	$-2.75 \times 10^{+00}$	$1.23 \times 10^{+00}$	9.37×10^{-01}	
6	-1.26×10^{-01}	-2.53×10^{-01}	-1.61×10^{-01}	3.92×10^{-02}	1.20×10^{-01}	$1.55 \times 10^{+00}$	8.74×10^{-01}	$1.16 \times 10^{+00}$	
7	-1.30×10^{-01}	-1.69×10^{-01}	2.73×10^{-01}	-9.72×10^{-02}	4.10×10^{-02}	-9.88×10^{-01}	-4.86×10^{-01}	-4.20×10^{-01}	
8	-1.70×10^{-01}	-2.73×10^{-01}	3.09×10^{-01}	6.93×10^{-02}	-3.07×10^{-01}	$2.19 \times 10^{+00}$	6.41×10^{-01}	6.57×10^{-01}	
9	5.08×10^{-01}	5.04×10^{-01}	2.60×10^{-01}	2.18×10^{-01}	-1.20×10^{-01}	9.73×10^{-02}	4.79×10^{-02}	$-1.80 \times 10^{+00}$	
10	-3.55×10^{-02}	-8.34×10^{-03}	-3.27×10^{-01}	5.66×10^{-02}	3.37×10^{-01}	$-1.22 \times 10^{+01}$	-6.69×10^{-01}	$-1.39 \times 10^{+00}$	

6. Conclusions

This study presents a finite element model to simulate the shale reservoir response in the gas production process for free and adsorbed gas within the shale matrix and the fracture. The mass conservation equation used to develop the gas transport equation includes both free and adsorbed gas. The adsorbed gas volume is calculated through Langmuir isotherms. The results show that the long term well performance is achieved during the gas production process and the existing adsorbed gas led to a stabilization in the production after an initial drop when the matrix elements reached critical desorption pressure.

Simulation results of Barnett Shale field show that the evolution of gas pressure strongly depends on the gas desorption process near the wellbore during gas production.

In addition, an ANN is created to forecast the gas production rates for different characteristics of the shale reservoirs. The number of hidden layers and neurons used in the ANN are one and ten, respectively. The results show that the developed ANN in this study predicts the gas rate precisely and these results led to the conclusion that the ANN can be used in some cases for saving computational time.

Author Contributions: Conceptualization, Software, Data creation, writing original draft R.A.A.; Methodology, Data creation, Writing—review & editing A.A. All authors have read and agreed to the published version of the manuscript.

Funding: This research work was funded by Institutional Fund Projects under grant no. (IFPIP: 423-145-1443).

Acknowledgments: This research work was funded by Institutional Fund Projects under grant no. (IFPIP: 423-145-1443). The authors gratefully acknowledge technical and financial support provided by the Ministry of Education and King Abdulaziz University, DSR, Jeddah, Saudi Arabia.

Conflicts of Interest: The authors declare that they have no conflict of interest.

References

1. Baihly, J.; Altman, R.; Malpani, R.; Luo, F. Shale gas production decline trend comparison over time and basins. In Proceedings of the SPE Annual Technical Conference and Exhibition, Florence, Italy, 19–22 September 2010. [\[CrossRef\]](#)
2. Darishchev, A.; de Nancy, E.N.; Lemouzy, P.; Rouvroy, P. On simulation of flow in tight and shale gas reservoirs. In Proceedings of the SPE Unconventional Gas Conference and Exhibition, Muscat, Oman, 28–30 January 2013. [\[CrossRef\]](#)
3. Tolmachev, O.M.; Urunov, A.A.; Muminova, S.N.; Dvoichenkova, G.P.; Davydov, I.A. Review of unconventional hydrocarbon resources: Production technologies and opportunities for development. *Min. Miner. Depos.* **2020**, *14*, 113. [\[CrossRef\]](#)
4. Alexander, T.; Baihly, J.; Boyer, C.; Clark, B.; Waters, G.; Jochen, V.; Le Calvez, J.; Lewis, R.; Miller, C.K.; Thaeler, J.; et al. Shale gas revolution. *Oilfield Rev.* **2011**, *23*, 40–57.
5. Alharthy, N.; Al Kobaisi, M.; Torcuk, M.A.; Kazemi, H.; Graves, R. Physics and modeling of gas flow in shale reservoirs. In Proceedings of the Abu Dhabi International Petroleum Conference and Exhibition, Abu Dhabi, United Arab Emirates, 11–14 November 2012. [\[CrossRef\]](#)
6. Anderson, D.M.; Nobakht, M.; Moghadam, S.; Mattar, L. Analysis of production data from fractured shale gas wells. In Proceedings of the SPE Unconventional Gas Conference, Pittsburgh, PA, USA, 23–25 February 2010. [\[CrossRef\]](#)
7. Andrade, J.; Civan, F.; Devegowda, D.; Sigal, R. Accurate simulation of shale-gas reservoirs. In Proceedings of the SPE Annual Technical Conference and Exhibition, Florence, Italy, 19–22 September 2010. [\[CrossRef\]](#)
8. Arthur, J.D. Hydraulic fracture for natural gas well of the Marcellus Shale. In Proceedings of the Ground Water Production Council Annual Forum, Cincinnati, OH, USA, 21–24 September 2008; Volume 88, pp. 15–20.
9. Asef, M.; Farrokhrouz, M. *Shale Engineering: Mechanics and Mechanisms*; CRC Press: Boca Raton, FL, USA, 2013; Volume 12, pp. 14–18.
10. Bello, R.O.; Wattenbarger, R.A. Modelling and analysis of shale gas production with a skin effect. *J. Can. Pet. Technol.* **2010**, *49*, 37–48. [\[CrossRef\]](#)
11. Soeder, D.J. The successful development of gas and oil resources from shales in North America. *J. Pet. Sci. Eng.* **2018**, *163*, 399–420. [\[CrossRef\]](#)
12. Berawala, D.S. Modelling of Gas Production from Tight Shale Formations: An Innovative Approach. Master's Thesis, University of Stavanger, Stavanger, Norway, 2015.
13. Knudsen, B.R. Production Optimization in Shale Gas Reservoirs. Master's Thesis, Institutt for Teknisk Kybernetikk, Trondheim, Norway, 2010.
14. Lee, S.J.; Kim, T.H.; Lee, K.S. Type curves for pressure transient analysis of horizontal wells in shale gas reservoirs. In Proceedings of the SPE Middle East Oil and Gas Show and Conference, Manama, Bahrain, 19–21 March 2013. [\[CrossRef\]](#)

15. Mengal, S.A. Accounting for Adsorbed Gas and Its Effect on Production Behavior of Shale Gas Reservoirs. Ph.D. Thesis, Texas A & M University, College Station, TX, USA, 2010.
16. Moghanloo, R.G.; Hosseini-pour, S.S. Mechanistic Modeling of Fluid Flow in Shale. In Proceedings of the SPE/AAPG/SEG Unconventional Resources Technology Conference, Denver, CO, USA, 25–27 August 2014. [\[CrossRef\]](#)
17. Olorode, O.M. Numerical Modeling of Fractured Shale-Gas and Tight-Gas Reservoirs Using Unstructured Grids. Ph.D. Thesis, Texas A & M University, College Station, TX, USA, 2012.
18. Olorode, O.; Wang, B.; Rashid, H.U. Three-dimensional projection-based embedded discrete-fracture model for compositional simulation of fractured reservoirs. *SPE J.* **2020**, *25*, 2143–2161. [\[CrossRef\]](#)
19. Azim, R.A. A poroelastic numerical model for simulation of hydraulic fracture propagation: Application to Upper Safa formation-Western Desert-Egypt. *Pet. Res.* **2020**, *5*, 39–51. [\[CrossRef\]](#)
20. Nguyen-Le, V.; Shin, H. Development of reservoir economic indicator for Barnett Shale gas potential evaluation based on the reservoir and hydraulic fracturing parameters. *J. Nat. Gas Sci. Eng.* **2019**, *66*, 159–167. [\[CrossRef\]](#)
21. Sesetty, V.; Ghassemi, A. Hydraulic fracture propagation in naturally fractured anisotropic shale. In Proceedings of the 52nd U.S. Rock Mechanics/Geomechanics Symposium, Seattle, WA, USA, 17–20 June 2018.
22. Ren, L.; Zhan, S.; Zhou, D.; Su, Y.; Wang, W.; Chen, M.; Jing, C.; Sun, J. Propagation simulation and structural characterization of multiple hydraulic fractures in naturally fractured unconventional hydrocarbon reservoirs. *J. Nat. Gas Sci. Eng.* **2020**, *83*, 103557. [\[CrossRef\]](#)
23. Ru, Z.; Hu, J.; Madni, A.S.; An, K. A study on the optimal conditions for formation of complex fracture networks in fractured reservoirs. *J. Struct. Geol.* **2020**, *135*, 104039. [\[CrossRef\]](#)
24. Zhang, H.; Sheng, J.J. Numerical simulation and optimization study of the complex fracture network in naturally fractured reservoirs. *J. Petrol. Sci. Eng.* **2020**, *195*, 107726. [\[CrossRef\]](#)
25. Vishkai, M.; Gates, I.D. Geomechanical characterization of naturally fractured formation. In Proceedings of the 52nd U.S. Rock Mechanics/Geomechanics Symposium, Seattle, WA, USA, 17–20 June 2018.
26. Qin, M.; Yang, D.; Chen, W.; Xia, X. Hydraulic fracturing network modeling based on peridynamics. *Eng. Fract. Mech.* **2021**, *247*, 107676. [\[CrossRef\]](#)
27. Kim, K.; Ju, S.; Ahn, J.; Shin, H.; Shin, C.; Choe, J. Determination of key parameters and hydraulic fracture design for shale gas productions. In Proceedings of the Twenty-fifth International Ocean and Polar Engineering Conference, Kona, HI, USA, 21–26 June 2015.
28. Li, Y.; Han, Y. Decline curve analysis for production forecasting based on machine learning. In Proceedings of the SPE Symposium: Production Enhancement and Cost Optimisation, Kuala Lumpur, Malaysia, 7–8 November 2017. [\[CrossRef\]](#)
29. Zhang, L. Fractured vertical wells in shale gas reservoirs without SRV. *Dev. Pet. Sci.* **2019**, *66*, 73–114. [\[CrossRef\]](#)
30. Nelson, B.; Belyadi, F.; Mashayekhi, A.; Aminian, K.; Ameri, S. Predicting long-term production behavior of the Marcellus shale. In Proceedings of the SPE Western North American and Rocky Mountain Joint Meeting, Denver, CO, USA, 16–18 April 2014. [\[CrossRef\]](#)
31. Bashir, M.O. Decline curve analysis on the woodford shale and other major shale plays. In Proceedings of the SPE Western Regional Meeting, Anchorage, AK, USA, 23–26 May 2016. [\[CrossRef\]](#)
32. Zuo, L.; Yu, W.; Wu, K. A fractional decline curve analysis model for shale gas reservoirs. *Int. J. Coal Geol.* **2016**, *163*, 140e8. [\[CrossRef\]](#)
33. Odi, U.; Bacho, S.; Daal, J. Decline curve analysis in unconventional reservoirs using a variable power law model: A Barnett shale example. In Proceedings of the SPE/AAPG/SEG Unconventional Resources Technology Conference, Denver, CO, USA, 25–27 July 2019. [\[CrossRef\]](#)
34. Wang, H. What factors control shale-gas production and production-decline trend in fractured systems: A comprehensive analysis and investigation. *SPE J.* **2017**, *22*, 562–581. [\[CrossRef\]](#)
35. Li, X.; Chan, C.W.; Nguyen, H.H. Application of the Neural Decision Tree approach for prediction of petroleum production. *J. Pet. Sci. Eng.* **2013**, *104*, 11–16. [\[CrossRef\]](#)
36. Clark, A.J.; Lake, L.W.; Patzek, T.W. Production forecasting with logistic growth models. In Proceedings of the SPE Annual Technical Conference and Exhibition, Denver, CO, USA, 30 October–2 November 2011. [\[CrossRef\]](#)
37. Klie, H. Physics-based and data-driven surrogates for production forecasting. In Proceedings of the SPE Reservoir Simulation Symposium, Houston, TX, USA, 23–25 February 2015.
38. Fulford, D.S.; Bowie, B.; Berry, M.E.; Bowen, B.; Turk, D.W. Machine learning as a reliable technology for evaluating time/rate performance of unconventional wells. *SPE Econ. Manag.* **2016**, *8*, 23–39. [\[CrossRef\]](#)
39. Nguyen-Le, V.; Shin, H. Artificial neural network prediction models for Montney shale gas production profile based on reservoir and fracture network parameters. *Energy* **2022**, *244*, 123150. [\[CrossRef\]](#)
40. Syed, F.I.; Alshamsi, A.; Dahaghi, A.K.; Neghabhan, S. Application of ML & AI to model petrophysical and geo-mechanical properties of shale reservoirs—A systematic literature review. *Petroleum* **2020**, *8*, 158–166.
41. Syed, F.I.; Alshamsi, M.; Dahaghi, A.K.; Neghabhan, S. Artificial lift system optimization using machine learning applications. *Petroleum* **2020**, *8*, 219–226. [\[CrossRef\]](#)
42. Alarifi, S.A.; Miskimins, J. A new approach to estimating ultimate recovery for multistage hydraulically fractured horizontal wells by utilizing completion parameters using machine learning. *SPE Prod. Oper.* **2021**, *36*, 468–483. [\[CrossRef\]](#)

43. Abdelgawad, K.; Elkatatny, S.; Moussa, T.; Mahmoud, M.; Patil, S. Real-time determination of rheological properties of spud drilling fluids using a hybrid artificial intelligence technique. *J. Energy Resour. Technol.* **2019**, *141*, 032908. [[CrossRef](#)]
44. Rumelhart, D.E.; Hinton, G.E.; Williams, R.J. Learning representations by back-propagating errors. *Nature* **1986**, *323*, 533–536. [[CrossRef](#)]
45. Caudill, M. Neural networks primer, Part III. *AI Expert* **1988**, *3*, 53–59.
46. Hush, D.R.; Horne, B.G. Progress in supervised neural networks. *IEEE Signal Process. Mag.* **1993**, *10*, 8–39. [[CrossRef](#)]
47. Guo, C. Flow Mechanisms and Numerical Simulation of Gas Production from Shale Reservoirs. Ph.D. Thesis, Missouri University of Science and Technology, Rolla, MO, USA, 2015.
48. Chang, O.C.Y. Integrated 3-Dimensional Modeling of Proppant Transport through Hydraulic Fracture Network in Shale Gas Reservoir. Ph.D. Thesis, The Pennsylvania State University, State College, PA, USA, 2016.